Journal of Alloys and Compounds 509 (2011) 9005–9009

Contents lists available at ScienceDirect

Journal of Alloys and Compounds

journal homepage: www.elsevier.com/locate/jallcom

Synthesis and characterization of cobalt-free $Ba_{0.5}Sr_{0.5}Fe_{0.8}Cu_{0.2}O_{3-\delta}$ perovskite oxide cathode nanofibers

Samaneh Shahgaldi[a,b,*], Zahira Yaakob[a,b], Dariush Jafar Khadem[a], Mojgan Ahmadrezaei[a,b], Wan Ramli Wan Daud[a]

[a] Fuel cell Institute, National University of Malaysia, 43600, UKM, Bangi, Selangor, Malaysia
[b] Department of Chemical and Process Engineering, Faculty of Engineering and Built Environment, University Kebangsaan Malaysia, 43600 UKM Bangi, Selangor, Malaysia

ARTICLE INFO

Article history:
Received 20 May 2011
Received in revised form 20 June 2011
Accepted 30 June 2011
Available online 7 July 2011

Keywords:
BSFC
Nanofibers
Cathodes
Electrospinning
Solid oxide fuel cell

ABSTRACT

The cobalt-free perovskite-oxide, $Ba_{0.5}Sr_{0.5}Fe_{0.8}Cu_{0.2}O_{3-\delta}$ (BSFC) is a very important cathode material for intermediate-temperature proton-conducting solid oxide fuel cells. $Ba_{0.5}Sr_{0.5}Fe_{0.8}Cu_{0.2}O_{3-\delta}$ nanofibers were synthesized for the first time by a sol–gel electrospinning. Process wherein a combination of polyvinylpyrrolidone and acetic acid was used as the spinning aid and barium, strontium, iron and copper nitrates were used as precursors for the synthesis of BSFC nanofibers. X-ray diffraction studies on products prepared at different calcination temperatures revealed a cubic perovskite structure at 900 °C. The temperature of calcination has a direct effect on the crystallization and surface morphology of the nanofibers. High porosity, and surface area, in addition to an electrical conductivity of 69.54 S cm^{-1} at 600 °C demonstrate the capability of BSFC nanofibers to serve as effective cathode materials for intermediate-temperature solid oxide fuel cells.

1. Introduction

Solid oxide fuel cells (SOFCs) are one of the most promising and efficient energy conversion devices with a variety advantages, including high efficiency, low pollution and fuel flexibility, these devices provide a direct exchange of chemical fuels into electrical power and are also practical from a commercial point of view [1–4]. Recently many publications have demonstrated the application of SOFCs for residential purposes revealing an increasing interest in this field. Great attention has focused on reducing the operating temperature of SOFCs from high temperature to intermediate temperatures [5–8]. The majority of studies focused on cobalt-based oxides with different compositions such as $Sm_{0.5}Sr_{0.5}CoO_{3-\delta}$ (SSC) [9], $Ba_{0.5}Sr_{0.5}Co_{0.8}Fe_{0.2}O_{3-\delta}$ [10], $Ba_{0.5}Sr_{0.5}(Co_{0.6}Zr_{0.2})Fe_{0.2}O_{3-\delta}$ [11], and $BaCo_{0.7}Fe_{0.3-y}Nb_yO_{3-\delta}$ [12]. This class of materials has several advantages including excellent performance, and prolonged lifetime [13]. However, these cobalt-based cathodes suffer from problems with high thermal expansion coefficients (TECs) and material losses due to evaporation [14,15]. The high cost of cobalt is another issue. As a result, the preparation of cobalt-free cathodes with a perovskite structure is highly desired. Wenping et al. [16] reported on the excellent performance of $BaZr_{0.1}Ce_{0.7}Y_{0.2}O_{3-\delta}$ and $Ba_{0.5}Sr_{0.5}FeO_{3-\delta}$ $Ce_{0.8}Sm_{0.2}O_{2-\delta}$ cathode materials. The effectiveness of $La_xSr_{1-x}FeO_{3-\delta}$, and $LaNi_{0.6}Fe_{0.4}O_{3-\delta}$ as cobalt free cathodes has also been investigated. All reported syntheses were performed using traditional solid-state reaction methods or with wet chemistry techniques such as modified citrate [17]. However, all of these methods are time consuming and produce non-homogeneous structures. Therefore, finding new methods is necessary for IT-SOFCs to overcome the problems of cost effectiveness and inefficient use of time. In recent years, the application of one-dimensional nanostructures, including nanowires and nanofibers, as cathode materials in IT-SOFCs has been the subject of intense research due to the reduction of device dimensions, potential nanomaterial properties due to the re-arrangement at the molecular level, and high surface areas [18–20]. There are a variety of methods for the synthesis of these nanostructures, such as laser ablation, chemical vapor deposition, solution deposition, and micro pulling method, but all these methods have the major disadvantages of being complicated, requiring significant time and high costs [21–23]. The electrospinning method, recently used for the production of ceramic nanofibers, overcomes nearly all of these disadvantages with its simplicity and cost effec-

* Corresponding author at: Administration Fuel cell Institute, National University of Malaysia, 43600, UKM, Bangi, Selangor, Malaysia. Tel.: +60 6 0389216065/60 176077347; fax: +60 6 0389216024.
E-mail addresses: Sami_shahgaldi@yahoo.com (S. Shahgaldi), zahira@eng.ukm.my (Z. Yaakob), d.khadem@eng.ukm.my (D.J. Khadem), mojgan2103@yahoo.com (M. Ahmadrezaei), wramli@vlsi.eng.ukm.my (W.R.W. Daud).

0925-8388/$ – see front matter © 2011 Elsevier B.V. All rights reserved.
doi:10.1016/j.jallcom.2011.06.117

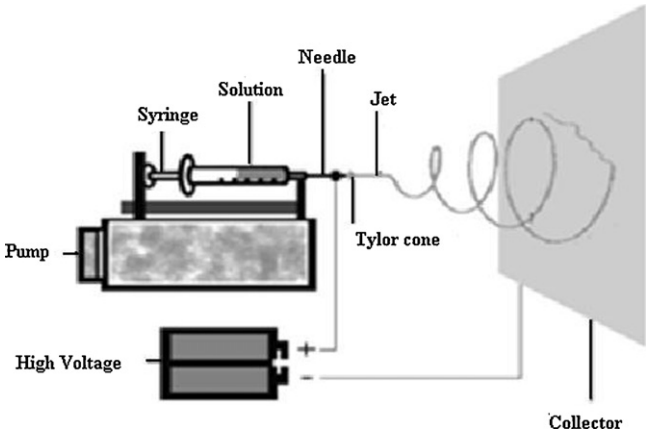

Fig. 1. Schematic diagram of the electrospinning process.

tiveness in the preparation of ceramic- or metal nanofibers with improved properties. This method includes three main steps. The first step is the preparation of a sol–gel using a suitable inorganic precursor and a proper polymer with suitable viscosity and homogeneity for electrospinning. Next electrospinning parameters such as the voltage, the distance between nozzle and collector and the feed rate are optimized in order to obtain nanofibers of polymer/precursor composites. Finally, the standardization of suitable calcination temperatures is performed to achieve the desired structure. In this work, we present the synthesis and characterization of $Ba_{0.5}Sr_{0.5}Fe_{0.8}Cu_{0.2}O_{3-\delta}$ (BSFC) nanofibers that serve as cathode materials for IT-SOFCs.

2. Materials and methods

Strontium nitrate, $Sr(NO_3)_2$ (99%), Sigma–Aldrich, Iron(III) nitrate nine hydrate, $Fe(NO_3)_3{\cdot}9H_2O$ (98.5%), Sigma–Aldrich, barium nitrate, $Ba(NO_3)_2$ (99%), Sigma–Aldrich, and copper(II) nitrate penta hydrate, Sigma–Aldrich, were used as the precursors. Acetic acid C_2H4O_2 (99.5%), Sigma–Aldrich, was used as the chelating agent. Polyvinylpyrrolidone (PVP), M_w: 1,300,000, Sigma–Aldrich, ethanol (100%), BDH, England, and deionized water were used as the spinning aid and solvents, respectively. All chemicals were used as purchased without further purification. For the synthesis of $Ba_{0.5}Sr_{0.5}Fe_{0.8}Cu_{0.2}O_{3-\delta}$/PVP nanofibers, the electrospinning method was used. In this method, an electrical potential was applied between a droplet of polymer–precursor solution at the end a spinneret and a grounded target. When the applied electric field exceeded the surface tension of the droplet, a charged jet of solution was ejected. Due to the bending instability, jet became longer and thinner until it was collected on a collector. Fig. 1 provides the schematic set up of the electrospinning apparatus. During the sol–gel process, stock solutions of $Sr(NO_3)_2$, $Fe(NO_3)_3$, $Ba(NO_3)_2$ and $Cu(NO_3)_2$ were premixed in stoichiometric ratios to produce the following molar ratios: Ba:Sr:Fe:Cu = 0.5:0.5:0.8:0.2. This mixture, containing a proper amount of acetic acid, was added drop-wise to a polymer solution. 1.5 g high molecular weight of polyvinylpyrrolidone in 11 ml ethanol was homogenized by stirring for 5 h. The prepared precursor/sol–gel solution was immediately drawn into a plastic syringe, equipped with a stainless steel needle. Next, an electrical potential was applied between the droplet of polymer/precursor in solution at the end of the spinneret nozzle and a grounded target. A DC voltage of 20 kV was applied using a high-voltage supply. The precursor solution was pumped at the rate of 1 ml/h using a syringe pump (new Eva pump systems, model NE = 1000). A piece of aluminum was placed 12 cm away from the top of needle, to collect the nanofibers. All electrospinning processes were performed at room temperature. The electrospun nanofibers were collected on a piece of aluminum foil. The prepared nanofibers were calcined at different temperatures in static air. The calcined oxide was crushed using a mortar and pestle. The BSFC fine powder were pelletized to form a 13 mm disc and later sintered by a standard atmosphere pressure sintering technique, which consists of pressing the cathode powder in a stainless steel die with uni-axial pressing pressures of 30, 35, and 40 MPa. The pellets were thereafter sintered at the temperature of 900 °C for 1 h in air for porosity measurements.

2.1. Characterization

Samples were subjected to thermogravimetric analysis (TGA), to determine the temperature of decomposition and phase change. The crystal structures of composites at different calcination temperatures were characterized by X-ray diffraction (XRD) using a Cu Kα 1 radiation source, with a primary monochromator of 40 kV and 40 mA, by varying 2θ from 10° to 80°. The texture and morphology of the nanofibers were examined using scanning electron microscopy (SEM) (ZEISS-EVOMA10), energy disperse X-ray spectroscopy (EDX) and transmission electron microscopy (TEM) methods. The surface area of nanofibers was measured using the Brunauer, Emmett Teller (AM1-200) (BET) method. Roughness, pore size and porosity were analyzed by atomic force microscopy (AFM). Electrical conductivity analysis was carried out using impedance spectroscopy with a Solarton (model SI 1286).

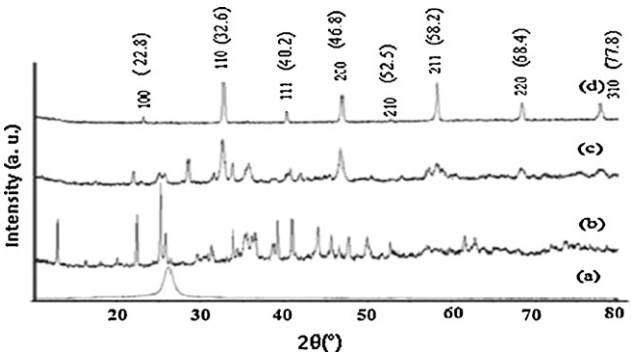

Fig. 2. XRD patterns of PVP/$Ba_{0.5}Sr_{0.5}Fe_{0.8}Cu_{0.2}O_{3-\delta}$ composite fibers at different calcination temperatures (a) electrospun PVP/$Ba_{0.5}Sr_{0.5}Fe_{0.8}Cu_{0.2}O_{3-\delta}$ (b) calcined at 500 °C (c) 700 °C (d) 900 °C.

3. Result and discussion

Fig. 2(a) provides the XRD pattern of the electrospun nanofibers, PVP/$Ba_{0.5}Sr_{0.5}Fe_{0.8}Cu_{0.2}O_{3-\delta}$, which shows only one peak characteristic of the polymer, and reveals the amorphous nature of the sample. The diffractograms obtained at increasing calcination temperatures reveal a perovskite phase structure for $Ba_{0.5}Sr_{0.5}Fe_{0.8}Cu_{0.2}O_{3-\delta}$, which is supported by the data reported by Zuo et al. [17]. The cubic perovskite structure appears above 700 °C. At this temperature, the diffraction peaks are weak, indicating the presence of an additional unknown phase, which may be due to Fe_3O_4, SrO, Cu_2O or BaO. Upon increasing the temperature further, the unknown peaks disappear, while the signals due to a single cubic perovskite structure remain. Sharp peaks in Fig. 2(d) reflect the formation of a well-ordered crystal with a perovskite structure at 900 °C, they also reveal that the BSFC is well crystallized at this temperature. Fig. 3 demonstrates the mechanism of decomposition and the production of the desired BSFC structure. From 30 to 175 °C, approximately 12.64% weight loss was observed due to the elimination of water, ethanol and bound moisture from the $Ba_{0.5}Sr_{0.5}Fe_{0.8}Cu_{0.2}O_{3-\delta}$/PVP spun fibers. The polymer backbone and the nitrates were removed below 450 °C. The two weight loss events from 180 to 370 °C and from 370 to 420 °C are due to the combustion of PVP and the decomposition of barium nitrate, respectively. Decomposition and weight loss ended at 900 °C producing the final oxide powder with a

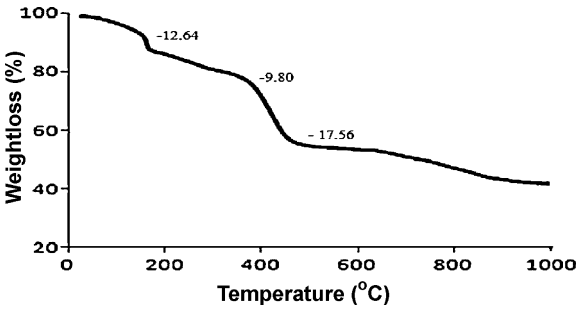

Fig. 3. TGA curves of thermal decomposition of $Ba_{0.5}Sr_{0.5}Fe_{0.8}Cu_{0.2}O_{3-\delta}$/PVP spun nanofibers.

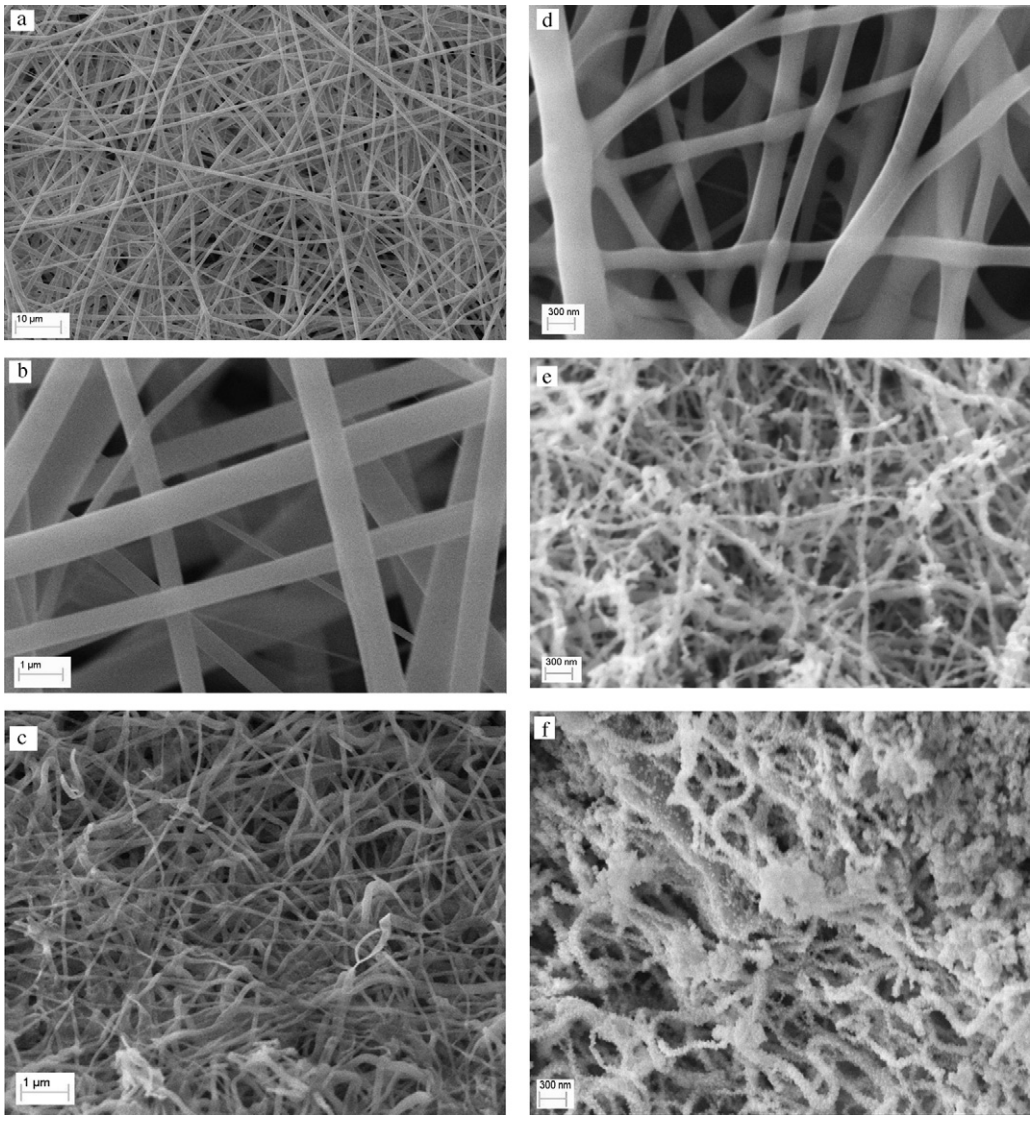

Fig. 4. Scanning electron microscope images of; (a and b) $Ba_{0.5}Sr_{0.5}Fe_{0.8}Cu_{0.2}O_{3-\delta}$/PVP composite fibers, micrograph of nanofibers calcined at (c and d) 500 °C (e) 700 °C (f) 900 °C.

perovskite structure. One of the main issues in cathode performance is related to the microstructure of the electrode material. Morphology, surface area, pore size and porosity of the electrode control the transport of gaseous species within the electrode, which directly affects the device performance [24]. The morphology of the electrospun polymer/composite and the calcined product of $Ba_{0.5}Sr_{0.5}Fe_{0.8}Cu_{0.2}O_{3-\delta}$/PVP nanofibers are shown in the SEM images in Fig. 4. The calcination of nanofibers has a direct effect on the surface morphology and the size of the sample. All SEM images were taken without a gold coating in order to see the real surface without the effect of gold. Fig. 4(a) shows the SEM images of electrospun polymer/precursor fibers prior to calcinations. The whole surface is covered with fibers without any beads. The fibers are smooth and uniform due to the amorphous nature of the polymer. The fibers are fairly long with an average diameter of 100–600 nm. As can be seen in Fig. 4(c and d) the SEM images of $Ba_{0.5}Sr_{0.5}Fe_{0.8}Cu_{0.2}O_{3-\delta}$/PVP calcined at 500 °C, reveal that the sample becomes a bit smooth due to the disappearance of the amorphous content and experiences a reduction in the diameter of the nanofibers, due to the loss of the polymer backbone. Upon increasing the calcination temperature, the polymer backbone becomes depleted to a greater extent. Fig. 4(e) shows the SEM images of the calcined forms of $Ba_{0.5}Sr_{0.5}Fe_{0.8}Cu_{0.2}O_{3-\delta}$/PVP at 700 °C. The fibers become completely rough and the diameter of fibers decreases to between 50 and 250 nm due to crystallization. By increasing the temperature of calcinations to 900 °C, the surface of the nanofibers becomes covered with particles. After the decomposition and removal of the polymer by calcination, an abrupt shrinkage within the fibers takes place causing significant tension at the pinning point (intertwined bonding in electrospun fibers exhibiting a pinning effect at the contact points between fibers); as a result, the length of fibers becomes smaller. These kinds of changes due to the calcination procedure cause a change in the crystal structure, which directly affects the morphology. To verify the presence of $Ba_{0.5}Sr_{0.5}Fe_{0.8}Cu_{0.2}O_{3-\delta}$ nanostructures in the fibers in significant quantities, we used (EDX). The EDX results for two different zones (Table 1) reveal the presence of the desired

Table 1
EDX results for BSFC nanofibers calcinated at 900 °C.

Sample	Ba (at%)	Sr (at%)	Fe (at%)	Cu (at%)
Zone 1	5.57	10.68	17.59	2.54
Zone 2	10.5	11.3	16.35	3.21

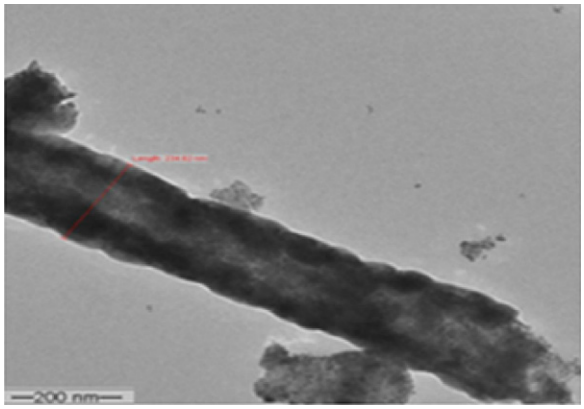

Fig. 5. TEM image of BSCF nanofibers.

nanomaterials and thus demonstrate the advantage of electrospinning in achieving all elements oriented perovskite materials. The morphology and exact structure of the BSFC nanofibers were examined using TEM. Fig. 5 provides the TEM image, which shows hollow BSFC nanofibers with a 200 nm diameter, composed of uniform nanoparticles with an average size of less than 20 nm. These nanoparticles join to create the BSFC nanofibers. Nanomaterials with a high surface area have shown improved cathode performance due to an increase in the concentration of active sites for oxygen reduction reaction (ORR). The specific surface area of the calcined nanofibers was characterized by N_2 adsorption using a BET instrument. This measurement reveals that BSFC nanofibers have a high surface area of 16.92 $m^2\,g^{-1}$, which makes this material applicable for intermediate-temperature solid-oxide fuel cells [24–26]. High porosity is the other important property for cathode materials in SOFC application. The pore size, roughness and porosity were characterized by using AFM as shown in Fig. 6. Table 2 provides these characteristics for BSFC nanofibers produced at different pressures. The porosity of the sample decreased with increasing the pressing pressures. Fig. 7 shows the FT-IR spectra of PVP and PVP/$Ba_{0.5}Sr_{0.5}Fe_{0.8}Cu_{0.2}O_{3-\delta}$ composite nanofibers calcined at different temperatures. Fig. 7(a) reveals absorption peaks at 3412, 2954, 1660, 1463 and 1290 cm^{-1} that are characteristic of –N–H, –C–H, –C=O and –CH_2 stretching frequencies of pure PVP fibers. By raising the calcination temperature from 500 °C to 900 °C, all of these peaks disappear due to the disappearance of the polymer (PVP) back-bone and new peaks appear at 560.70, 1632 and 3400 cm^{-1} assigned to Cu–O stretching. The electrical conductivity versus temperature of a dense pellet of BSFC nanofibers in air sintered at 900 °C is shown in Fig. 8. By increasing the temperature, the conductivity increases until 600 °C, upon which time it reaches a maximum value of 69.54 S cm^{-1}. Beyond this temperature, conductivity begins to decrease (pseudometallic) due to loss of lattice oxygen and also the reduction of iron ions in B-site at elevated temperatures [26]. Previously, similar work carried out by Zhao et al. [27] reported conductivity of 57 S cm^{-1} at 600 °C. However, they synthesized BSFC by auto ignition process at different condition. By these comprehensive characteristic of BSFC nanofibers, we hope to open new generation of cathodes material in SOFCs application (Figs. 7–8).

Table 2
AFM analysis of BSFC pellets with different pressures.

BSFC nanofibers pellet	Pore size (nm)	Average roughness	Porosity (%)
BSFC 40	289	12.56	34.5
BSFC 35	199	19.05	39.9
BSFC 30	144	27.86	41.8

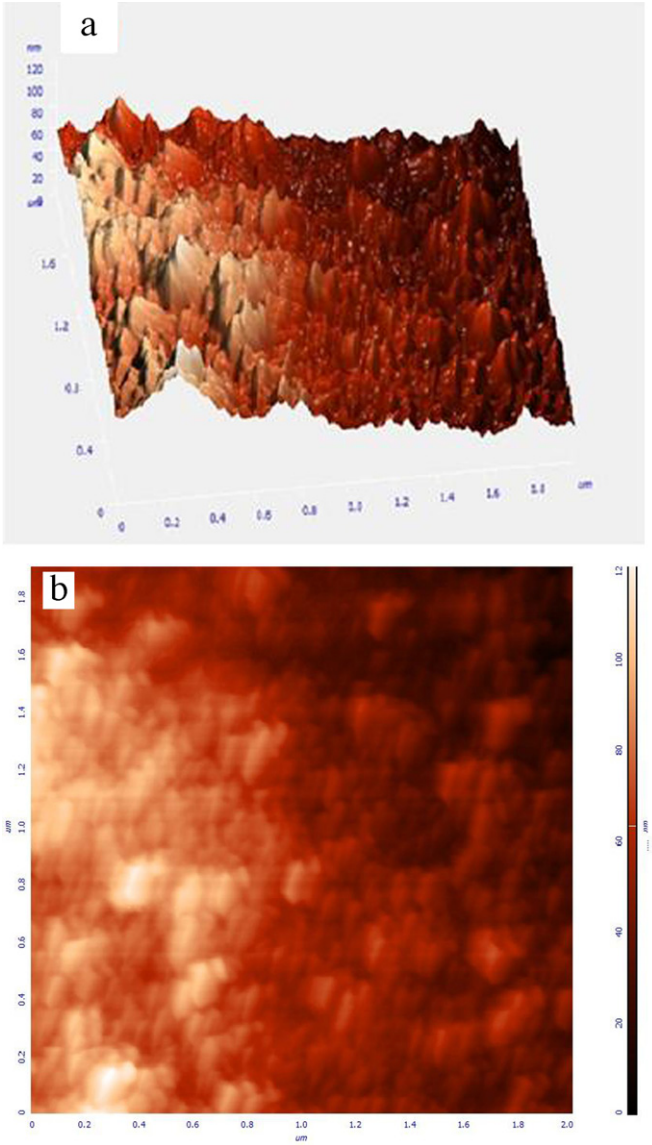

Fig. 6. 2D and 3D AFM images of BSFC nanofibers.

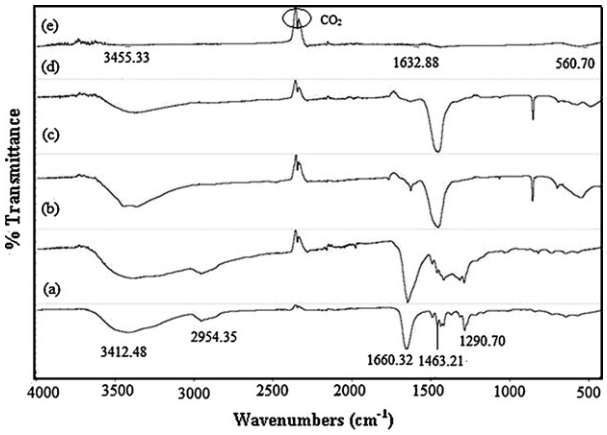

Fig. 7. FT-IR spectra of PVP/$Ba_{0.5}Sr_{0.5}Fe_{0.8}Cu_{0.2}O_{3-\delta}$ composite fibers produced at different calcination temperatures. (a) PVP alone (b) PVP/$Ba_{0.5}Sr_{0.5}Fe_{0.8}Cu_{0.2}O_{3-\delta}$ (c) 500 °C (d) 700 °C (e) 900 °C.

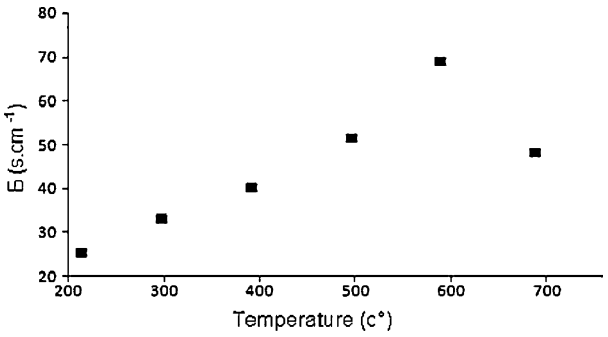

Fig. 8. Electrical conductivity of BSFC nanofibers.

4. Conclusion

In this study, cobalt-free, perovskite oxide nanofibers were successfully prepared for the first time, using $Ba_{0.5}Sr_{0.5}Fe_{0.8}Cu_{0.2}O_{3-\delta}$/PVP composites, this was achieved through the sol–gel assisted electrospinning method followed by calcination, which used metal salts as precursors and polyvinylpyrrolidone as the carrier. High yield, simplicity and cost effectiveness are the main advantages of the method. Hollow BSFC nanofibers with a diameter ranging from 50 to 250 nm were formed on the collector. By increasing the calcinations temperature to 900 °C, cubic perovskite oxides with high specific surface area of around 16.92 $m^2\,g^{-1}$ were obtained. The high conductivity of BSCF nanofibers is another advantage of this cathode material. It is expected that electrospun high porosity BSFC nanofibers have the potential to serve as cobalt-free cathode materials in intermediate temperature solid-oxide fuel cells due to their improved properties.

Acknowledgment

The authors would like to thank the Fuel Cell Institute of National University of Malaysia for its support under the UKM-AP-TK-05-2009 grant.

References

[1] A. Endo, M. Ihara, H. Komiyama, K. Yamad, Solid State Ionics 86–88 (1996) 1191–1195.
[2] J.A. Kilner, R.A. De Souza, I.C. Fullarton, Solid State Ionics 86–88 (1996) 703.
[3] N.P. Brandon, S. Skinner, B.C.H. Steele, Annu. Rev. Mater. Res. 33 (2003) 183–213.
[4] L. Yang, S. Wang, K. Blinn, M. Liu, Z. Liu, Z. Cheng, M. Liu, J. Sci. 326 (2009) 126–129.
[5] H. Daisuke, T. Atsuko, T. Shiny, H. Takashi, S. Mitsuru, Solid State Ionics 176 (2005) 881–887.
[6] A. Demin, P. Tsiakaras, Int. J. Hydrogen Energy 26 (2001) 1103–1108.
[7] J.M. Serra, H.P. Buchkremer, J. Power Sources 172 (2007) 768–774.
[8] R.T. Leah, N.P. Brandon, P. Aguiar, J. Power Sources 145 (2005) 336–352.
[9] C.R. Xia, W. Rauch, F.L. Chen, M.L. Liu, Solid State Ionics 149 (2002) 11–19.
[10] Y. Zhang, J. Liu, X. Huang, Z. Lu, W. Su, Solid State Ionics 179 (2008) 250–255.
[11] X. Meng, B. Meng, X. Tan, N. Yang, Z.F. Ma, Mater. Res. Bull. 44 (2009) 1293–1297.
[12] C. Zhu, X. Liu, C. Yi, L. Pei, D. Yan, J. Niu, D. Wang, W. Su, Electrochem. Commun. 11 (2009) 958–961.
[13] M. Darab, M.S. Toprak, G.E. Syvertsen, M. Muhammed, J. Electrochem. Soc. 156 (2009) 139–143.
[14] B. Wei, Z. Lu, X.Q. Huang, M.L. Liu, N. Li, W.H. Su, J. Power Sources 176 (2008) 1.
[15] H.H. Wang, C. Tablet, A. Feldhoff, J. Caro, Adv. Mater. 17 (2005) 1785.
[16] W. Sun, Z. Shi, Sh. Fang, L. Yan, Z. Zhu, W. Liu, Int. J. Hydrogen Energy 34 (2010) 7925–7929.
[17] W. Zhou, R. Ran, Z. Shao, J. Power Sources 192 (2009) 231–246.
[18] W. Nuansin, S. Maensiri, Adv. Sci. Technol. 45 (2007) 735–740.
[19] S. Maensiri, W. Nuansin, J. Klinkaewnarong, P. Laokul, J. Khemprasit, J. Colloid Interface Sci. 297 (2006) 578.
[20] X.Q. Shen, J. Xiang, F.Z. Song, M.Q. Liu, Appl. Phys. A 99 (2010) 189–195.
[21] Y. Ikezawa, K. Nishimura, H. Uchilda, M. Inoue, J. Magn. Magn. Mater. 272–276 (2004) 1690–1691.
[22] V.I. Chani, A. Yoshikava, Y. Kuwano, K. Hasegawa, T. Fukuda, J. Cryst. Growth 204 (1999) 155–162.
[23] P.J. Hull, J.L. Hutchison, O.V. Salata, P.J. Dobson, Adv. Mater. (1997) 413.
[24] J. Peña-Martínez, D. Marrero-López, J.C. Ruiz-Morales, P. Núñez, C. Sánchez-Bautista, A.J. Dos Santos-García, J. Canales-Vázquez, Int. J. Hydrogen Energy 34 (2009) 9486–9495.
[25] M. Ghouse, Y. Al-Yousef, A. Al-Musa, M.F. Al-Otaibi, Int. J. Hydrogen Energy 35 (2010) 9411–9419.
[26] M. Bellino, J. Sacanell, D. Lamas, A. Leyva, N. Walsöe de Reca, J. Am. Chem. Soc. 129 (2007) 3066.
[27] L. Zhao, B. He, X. Zhang, R. Peng, G. Meng, X. Liu, J. Power Sources 195 (2010) 1859–1861.